Title

Optimization of echo-enabled harmonic generation toward coherent EUV and soft X-ray free-electron laser at NSLS-II

Journal

Scientific Reports, 12(1)

ISSN

2045-2322

Authors

Yang, X

Penn, G

Yu, LH

et al.

Publication Date

2022-06-01

DOI

10.1038/s41598-022-13702-3

Peer reviewed

Optimization of Echo-Enabled Harmonic Generation toward coherent EUV and soft X-ray free-electron laser at NSLS-II

X. Yang[1*], G. Penn[2*], L. H. Yu[1], V. Smaluk[1], T. Shaftan[1]
[1]*National Synchrotron Light Source II, Brookhaven National Laboratory, Upton, NY 11973, USA*
[2]*Lawrence Berkeley National Laboratory, Berkeley, CA 94720, USA*
*corresponding.xiyang@bnl.gov, *corresponding.gepenn@lbl.gov

ABSTRACT

Prebunching via echo-enabled harmonic generation (EEHG) is an efficient way to reduce the radiator length and improve the longitudinal coherence as well as output stability in storage-ring-based free-electron lasers (FELs). We propose a conceptual design which uses two straight sections to seed coherent extreme-ultraviolet (EUV) and soft X-ray emission with nearly MHz repetition rate. To take the large energy spread (10^{-3}) of a storage ring into account and utilize the existing bending magnets between the two straight sections as the first chicane, we implement a special modeling tool, named EEHG optimizer. This tool has been successfully applied to maximize the prebunching with a reasonably low energy modulation, thereby generating intense coherent X-ray pulses within a short undulator length (a few meters) limited by the available space of a storage ring. Numerical simulations confirm that the optimized EEHG parameters can be directly applied to generate a 10 MW scale peak power with fully coherent ultrafast EUV to soft X-ray pulses based on the NSLS-II parameters. This method can be easily extended to other types of diffraction-limited storage rings.

INTRODUCTION

Compared to conventional high-gain harmonic generation (HGHG)[1-4], the echo-enabled harmonic generation (EEHG) scheme is significantly less sensitive to energy spread, which is typically large in storage rings. Recently, to overcome such large energy spread, the use of transverse gradient undulators (TGUs) has been proposed for a high-gain short wavelength FEL driven by a diffraction-limited synchrotron light source[5]; however, this approach requires bunches to be diverted into an additional ring with its own rf cavities. Since the EEHG seeding option requires no change of the storage ring lattice and is fully compatible with other beamlines, the compact design currently studied could enable synchrotron light source based free-electron lasers (FELs) to produce intense coherent radiation pulses with short durations[6-11]. Such fully coherent ultrafast photon pulses up to the carbon K-edge offers unique opportunities to conduct high resolution spectroscopy on organic materials that are important in environmental science, medicine, biology, and bio-renewable energy materials[12]. Also, extending the pump-probe approach known from ultraviolet/visible spectroscopy to shorter wavelengths allows detailed studies of excited-state dynamics in organic molecules or biomolecular structures on a nanosecond to femtosecond time scale. Optical pump soft X-ray probe spectroscopy is a relatively new approach to detect and characterize optically dark states in organic molecules, to explore exciton dynamics, or to observe transient charge transfer states. Recent developments on extreme-ultraviolet (EUV) and soft X-ray sources based on EEHG storage-ring FELs open new opportunities for studying excited-state dynamics in organic molecules, together with the tremendous increase of computing power, allows understanding the excited-stage behavior even of very complex organic molecules in more detail[13,14].

Driven by those scientific applications, the implementations of EEHG at the NSLS-II and the future diffraction-limited upgrade (NSLS-IIU)[15] are presently studied as an option to improve

the longitudinal coherence and output stability, toward fully coherent storage ring-based FELs. To take the unique challenge and characteristics of storage-ring-based EEHG FELs into account, we have developed a modeling tool, named EEHG optimizer. This toolkit has been successfully applied to the NSLS-II storage ring with an up to two orders of magnitude improvement of the spectral brightness regarding the 12 nm wavelength. This scheme can be easily extended to any other type of 4th generation diffraction-limited storage ring[15-20].

RESULTS

I. DEVELOPMENT OF STORAGE-RING-BASED EEHG OPTIMIZER

1.1 Tuning Echo Parameters

Starting with two seed lasers, we aim to produce a large harmonic through EEHG[21,22]. There are two modulation stages, each followed by a chicane or a dogleg[23]. These stages are labeled as 1 and 2. In a storage-ring-based EEHG seeding scheme, since the first chicane is determined by the bending magnets (BM) between two straights, it is convenient to take the momentum compaction R_{56} as a fixed quantity[23], denoted R_1. Here, the momentum compaction, defined as the derivative of normalized path length difference to normalized momentum ($\frac{p}{L}\frac{dL}{dp}$), is a measure of the momentum dependence of path length[23]. The convention used here is that a typical chicane of four bend magnets has a negative value of R_{56}. The second parameter to choose is the energy modulation of the first stage, η_{M1}. It may also be characterized by its value relative to the energy spread (see below). Fixing a different parameter such as the second R_{56} involves coupling with other parameters and is difficult to select an optimal value without detailed analysis.

The output wavelength, λ_r, is also an important criterion since it can result from microbunching at that wavelength or a sub-harmonic. Together with the wavelengths of external lasers and thus the modulations, these choices will determine the parameters in stage 2, with two possible solutions (see Section 1.3). Given the external laser wavelength λ_1 and λ_2, the output wavelength ideally has the form:

$$k_r = p \cdot k_1 + m \cdot k_2 \quad (1)$$

where $k_{1,2} = 2\pi/\lambda_{1,2}$, and m and p must be integers. Usually, we assume λ_1, λ_2, and thus λ_r are integer harmonics of a single wavelength, although it may not matter too much either way. This constrains the choices of possible output wavelengths. Often m is small, so $p \gg 1$ roughly determines the wavelength. We can treat m as an additional choice (or knob) related to the dominant wavelength of the bunched beam, which is close to $m \cdot \lambda_r$. The other main parameter is the energy spread, σ_η, which is fixed in a storage-ring-based FEL (e.g., 10^{-3} for NSLS-II) by the equilibrium between radiation damping and energy diffusion.

1.2 Appling Optimizer to NSLS-II

Based upon the procedures described in the METHOD section, we have implemented an EEHG optimizer for the purpose of tuning all important parameters toward the ideal performance of an EEHG beamline in a synchrotron light source.

To cover the soft X-ray spectrum up to the carbon K-edge (4.13 to 12.4 nm), the harmonics of EEHG regarding the wavelength of stage 1, $\lambda_1 = 800\,nm$, should be optimized in the range of 65 to 191. As example, we apply our newly developed storage-ring-based EEHG optimizer to the NSLS-II lattice. Since the EEHG layout will be discussed in Section II with

greater detail, we only show the maximum bunching (b), the final root mean square (RMS) energy spread (ΔE_{tot}), the C parameter (defined by Eq. 5 in METHOD section), the optimal momentum compaction of chicane 2 with an opposite sign ($-R_2$), the powers of laser 1 (P_{laser1}) and laser 2 (P_{laser2}) as functions of the harmonic (y axis) and the energy modulation of stage 1 (x axis) as the contour plots in Figs. 1a to 1f, respectively. The C parameter decreases with the increase of the modulation amplitude and is about two orders of magnitude smaller than the two terms, $k_r R_2$ and $k_1 R_1$, which are both around $7.5 \cdot 10^4$. The reasons why we choose the harmonic and the energy modulation of stage 1 as the input variables are:

- Once the harmonic, the momentum compaction of chicane 1 (R_1), and the energy modulation of stage 1 (A_1) are fixed, the Bessel functions with the maximal values of the bunching determine the optimal values of the momentum compaction of chicane 2 and the energy modulation of stage 2.
- The momentum compaction of chicane 1 is fixed by the momentum compaction of the storage ring lattice.
- The upper and lower limits of harmonics are determined by the user interested spectrum.
- The energy modulation of stage 1 must be optimized for maximum coherent radiation (CR) power. This goal can be achieved via maximizing the prebunching as well as mitigating the de-bunching effect through the radiator (see section III for details).

Prebunching produced by EEHG is quite different from that produced from HGHG[1-4]. From harmonic 65 to harmonic 191, only about 30% decrease in the bunching factor is observed, as shown in Fig. 1g. There is still a significant amount of bunching (0.08) at harmonic 191 with A_1=5. From Fig. 1h, we see that the maximal value of the bunching increases linearly with A_1 when A_1 is smaller than 2. When A_1 becomes larger than 3, the growth of maximal values slows down. This feature turns the storage-ring-based EEHG application into an attractive option via improving the longitudinal coherence with a moderate energy modulation. A small energy modulation is desired since the relative energy spread of a storage ring is a few to ten times larger compared to 10^{-4} often associated with linear-based accelerators. It is evident that there are two optimal solutions with the same bunching but slightly different values of R_2 and A_2, as shown in Fig. 1i.

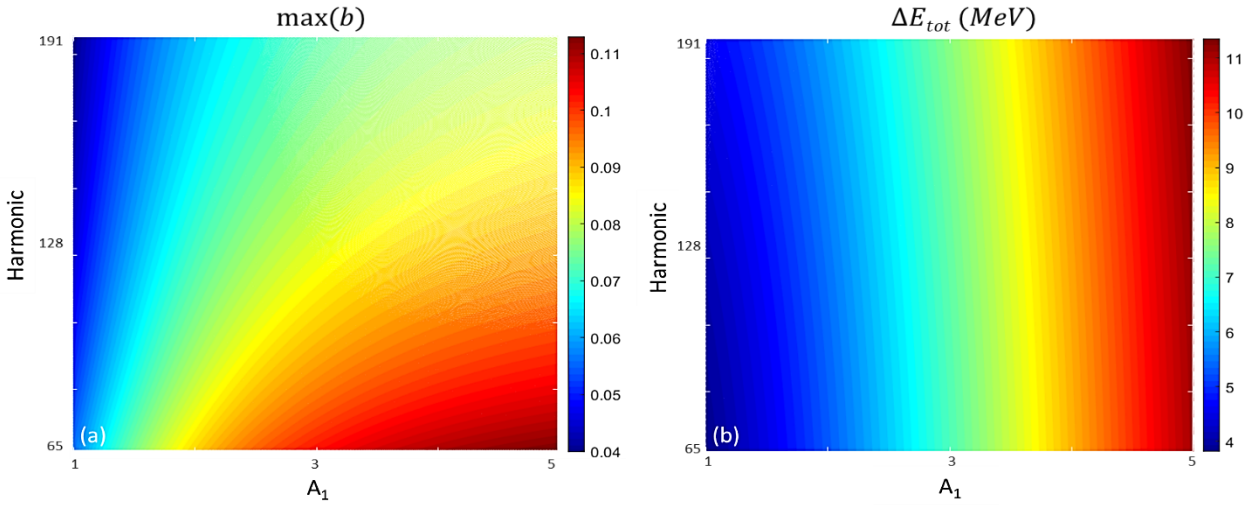

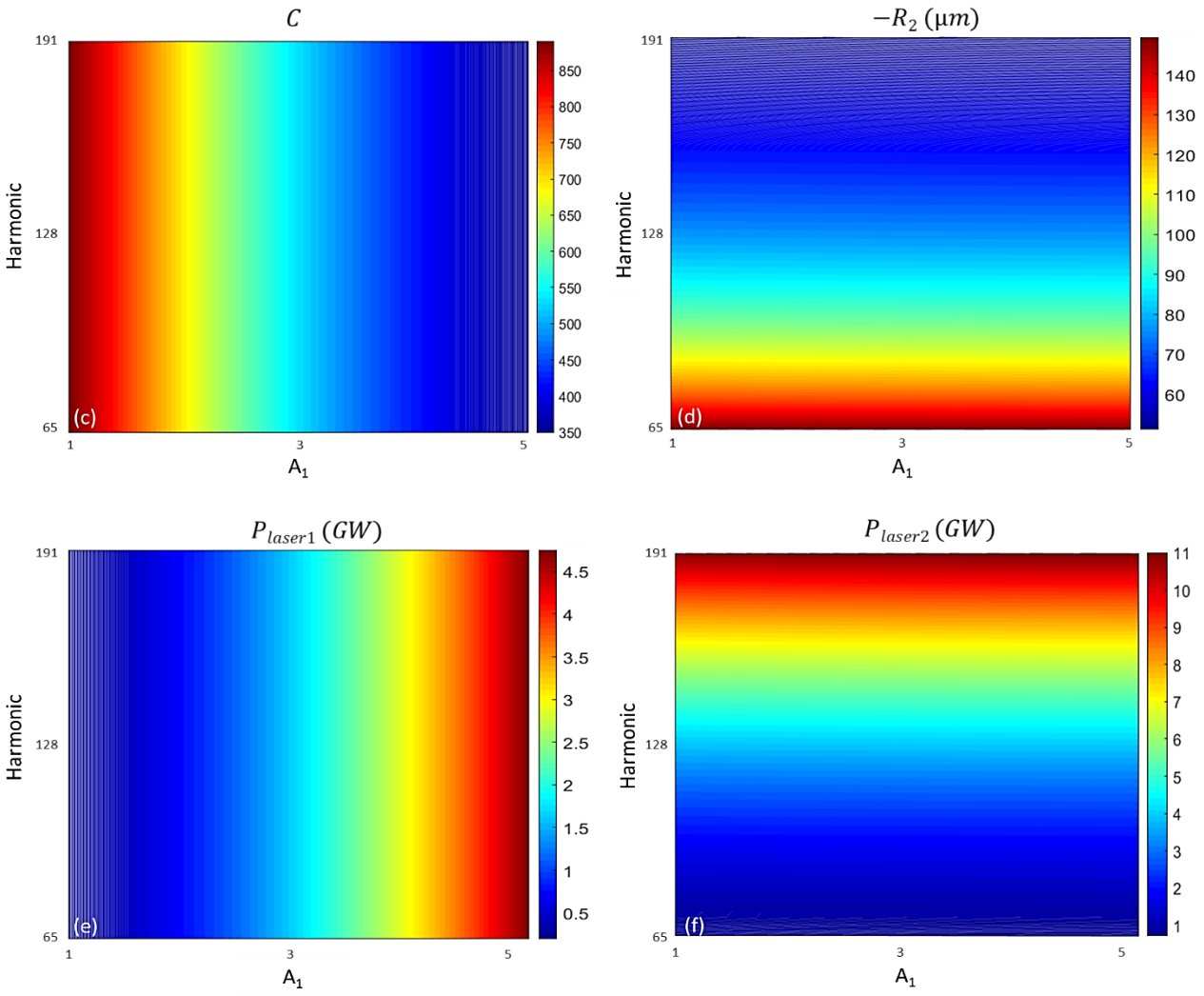
C
$-R_2\ (\mu m)$
$P_{laser1}\ (GW)$
$P_{laser2}\ (GW)$
Harmonic
A_1
(c)
(d)
(e)
(f)
191
128
65
1
3
5
850
800
750
700
650
600
550
500
450
400
350
140
130
120
110
100
90
80
70
60
4.5
4
3.5
3
2.5
2
1.5
1
0.5
11
10
9
8
7
6
5
4
3
2
1

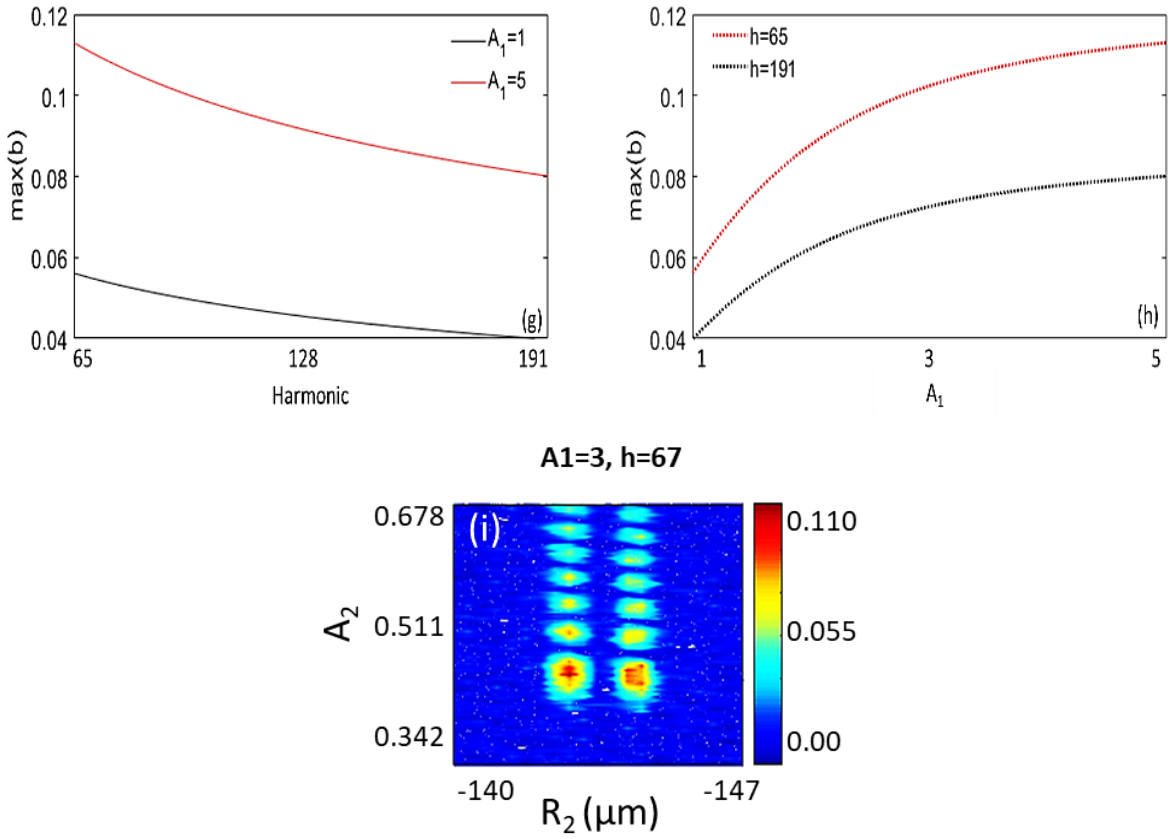

Figure 1. (a) The maximum bunching, (b) the final RMS energy spread, (c) the *C* parameter defined by Eq. 5 in METHOD section, (d) the optimal momentum compaction of chicane 2, (e) the powers of laser 1 and (f) laser 2 as functions of the harmonic (y axis) and the energy modulation of stage 1 (x axis) are shown as contours, respectively. R_2 of chicane 2 should have the opposite sign relative to R_1 of chicane 1, which is +9.6 mm, hence, we plot the absolute value of R_2. (g) Maximum bunching vs harmonic number is plotted for two cases: A_1=1 (black) and A_1=5 (red). (h) Maximum bunching vs modulation amplitude of stage 1 is plotted for two cases: harmonic 65 (red) and 191 (black). (i) With a fixed $A_1=3$ and $R_1=+9.6$mm at harmonic 67, prebunching as functions of the energy modulation of stage 2 (A_2) and the momentum compaction of chicane 2 (R_2) is shown as the contour plot. It is evident that there are two optimal solutions with slightly different values of R_2 and A_2.

II. DESIGING AN EEHG FEL IN A SYNCHROTRON LIGHT SOURCE

2.1 Design Strategy

EEHG scheme enables the possibility for synchrotron light source based FELs to produce intense CR pulses with short durations. To achieve fully coherent storage ring-based FELs[15,24,25], the implementations of EEHG at the NSLS-II and the future upgrade diffraction-limited NSLS-IIU are presently studied. We plan to use two straight sections for seeding the coherent EUV and soft X-ray emission at the repetition rate up to MHz.

There are a few important issues associated with the design of the EEHG beamline in the NSLS-II case[25]. They are:

- BM section between two straight sections provides the momentum compaction R_1 of the first chicane with $+9.6\,mm$.
- Modulation stage 1 and 2 must be separated by the BM section between the two straight sections.

- To maximize the CR power, the radiator needs to be positioned in the short straight section where the beta functions are small, hence the beam sizes are small.
- Large energy spread in RMS (10^{-3}) limits the highest harmonic (e.g., 191 for carbon K-edge at 4.13 nm).
- The wavelength of laser 1 is fixed to 800 nm.
- The wavelength of laser 2 (λ_2 = 400 nm) is chosen to be the second harmonic of laser 1.
- Selecting different parts of an electron bunch may extend the repetition rate from ~10 kHz up to 1 MHz.

Comparing λ_2 = 400 nm with λ_2 = 800 nm, the modulation amplitude of stage 2 can be reduced to half while keeping the same bunching factor regarding a specific harmonic. This can greatly benefit prebunching at high harmonics, with less energy modulation, thus, less beam heating. Also, repetition rate can surpass the limit that is set by the radiation damping time of a storage ring, ~ 10 ms for the NSLS-II[25]. The original 10 kHz repetition rate ($1/10\,ms \times 100\,bunches/turn$) can be increased by a factor up to 100, which is approximately determined by the ratio of the electron bunch length and the modulated slice duration.

For this wavelength range, wake fields and stochastic energy scatter should not significantly impact the achieved bunching parameter.

2.2 Design of EEHG Beamline

A schematic layout of the EEHG beamline at the NSLS-II storage ring is shown in Fig. 2. Stage 1, including modulator 1 and laser 1, is positioned downstream of the long straight section. Instead, stage 2, including modulator 2, laser 2, and chicane 2, locates upstream of the short straight section. The radiator is positioned downstream of the short straight section. The resonant wavelengths for modulator 1 and modulator 2 are 800 nm and 400 nm, respectively. The resonant wavelength of the radiator must cover the entire spectral range up to the carbon K-edge, from 4.13 nm to 12.4 nm, via varying the undulator gap.

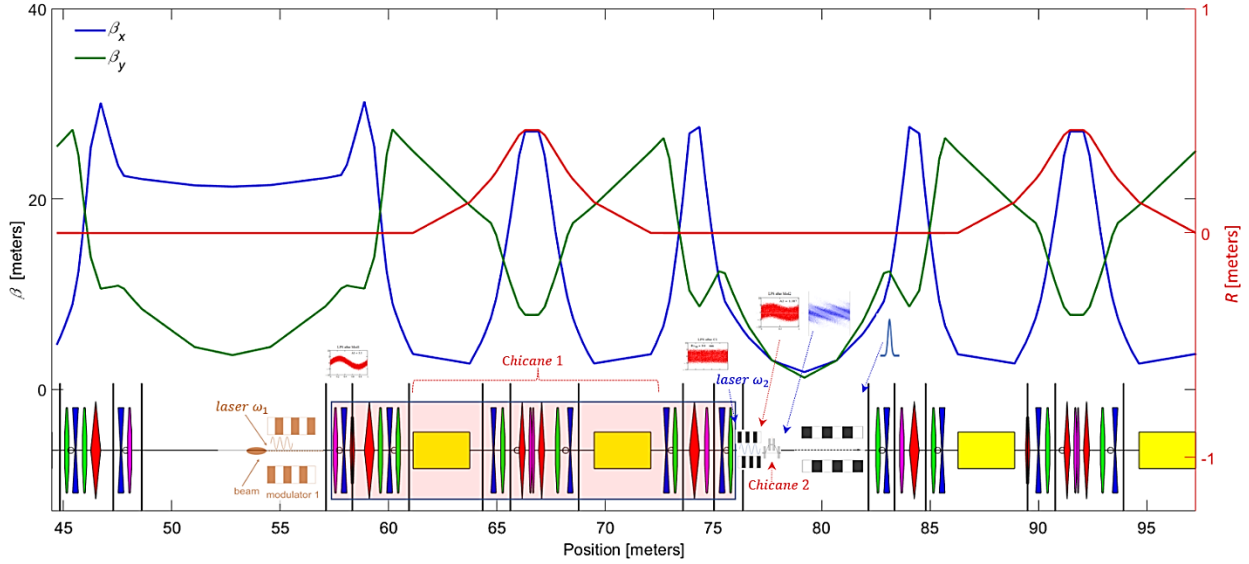

Figure 2. Schematic layout of EEHG at NSLS-II. Horizontal and vertical beta functions are plotted as the blue and the green curves, respectively. Horizontal dispersion is plotted as the red curve of the secondary y axis.

The required seed laser power scales as the square of energy modulation amplitude and beam size, and the inverse square of undulator K parameter and length. To minimize the seed laser power of stage 2, the modulator 2 will be placed in the short straight section where the beta functions are small. The short straight section has a limited usable space, around 5 m, and will be occupied by three main elements of the EEHG beamline, including modulator 2, chicane 2, and the radiator. The magnetic field as a function of the undulator gap for a permanent magnet undulator (PMU) is given by

$$B_0\left(gap,\lambda_u,B_{max},M,h_B\right)=2\cdot B_{max}\cdot\frac{M}{\pi}\cdot\sin\left(\frac{\pi}{M}\right)\cdot\left(1-e^{\frac{-2\cdot\pi\cdot h_B}{\lambda_u}}\right)\cdot e^{\frac{-\pi\cdot gap}{\lambda_u}}, \tag{2}$$

where M=4 is the number of magnets per period, $h_B(5\,cm)$ is the height of magnets, and B_{max} is the maximum B field[26]. The K parameter as a function of the gap is given by

$$K\left(gap,\lambda_u,B_{max}\right)=\frac{B_0\left(gap,\lambda_u,B_{max},M,h_B\right)\cdot\left(e_0\cdot\lambda_u\right)}{2\cdot\pi\cdot\left(m\|0c\right)}. \tag{3}$$

The EEHG beamline parameters are listed in Table 1. The turnabilities of the minimum and maximum wavelengths are set by the maximum and minimum allowed undulator gaps, respectively. To avoid the radiation damage, the maximum B field is limited to be less than $1.3\,T$. For the radiator with the period of 6.4 cm and the maximum B field of $0.90\,T$, the gap can be allowed to vary in the range of 6 to 50 mm. The vertical red line with arrow ends in Fig. 3a indicates the entire spectrum of the carbon K-edge. K parameter vs gap is shown in Fig. 3b. To cover the wavelength range of 4.13 to 12.4 nm, the gap needs to be varied in the range of 20.9 down to 8.5 mm, corresponding to K values of 3.50 and 6.38, respectively.

					Gap (mm)			Resonant wavelength (nm)			K (T·cm)		
Eelement	Period	Length	unit	B_{max} (T)	min	max	operation	min	max	operation	min	max	operation
MOD 1	*64*	256	cm	0.34			17.3			800			13.05
MOD 2	*20*	100	cm	0.9			24.0			400			16.55
Radiator	*6.4*	352	cm	0.9	8.5	21	[8.5 21]	4.13	12.4	[4.13 12.4]	3.5	6.38	[3.5 6.38]

Table 1. The parameters of modulator 1, modulator 2, and radiator are listed, including period, total length, maximum B field, minimum, maximum, and operational gaps, and K parameter.

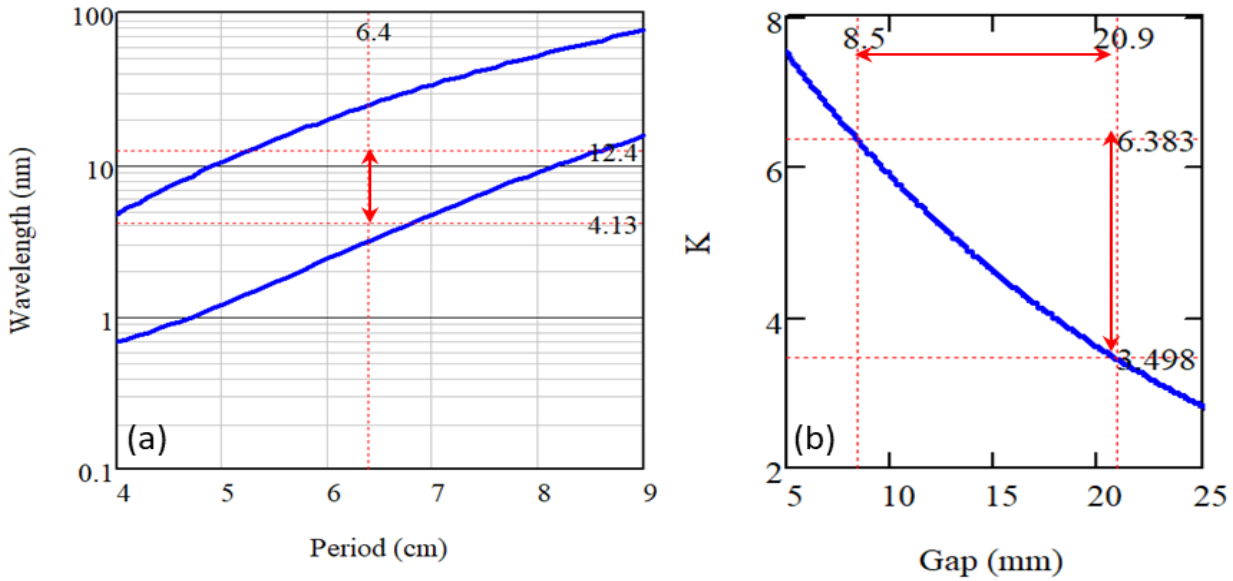

Figure 3. For the radiator with the period of 6.4 cm and the maximum B field of 0.90 T, the gap can be varied in the range of the minimum 6 mm to the maximum 50 mm. (a) (left) Wavelength vs undulator period is plotted with the minimum gap (upper blue line) and the maximum gap (lower blue line). The wavelength in the range of [4.13 12.4] nm determines the optimum period of 6.4 cm. (b) (right) Modulator *K* parameter vs gap. The radiation wavelengths ([4.13 12.4]) nm corresponds to the gap between 20.9 mm to 8.5 mm and the *K* parameter between 3.5 and 6.4.

III. Simulation for Generating Intense EUV and Soft X-ray Radiation

One expects that a smaller energy modulation becomes more critical for long undulators. A small energy modulation begins with a low energy spread as well as a small prebunching. The radiation power and the bunching are continuously growing through the undulator, eventually reaching the saturation power determined by the FEL Pierce parameter. Instead, a large energy modulation is often associated with a large prebunching, hence, allows a much faster growth of the CR power, even within a short undulator distance (e.g., a few meters). This is the case of the storage-ring-based EEHG FEL. The radiator length is limited to be ≤ 3.5 m in the NSLS-II.

The purpose of optimization becomes searching an optimal energy modulation, which provides the fastest growth of the CR power and simultaneously mitigates the effect of the rapid de-bunching induced by the large energy spread ($2 \cdot N_u \cdot \frac{\Delta E_{tot}}{E} \approx 2 \cdot \frac{3.52\,m}{0.064\,m} \cdot 2 \cdot 10^{-3} \approx 0.2$ for the nominal energy modulation). Here, N_u refers to the number of undulator periods in the radiation stage. The optimal energy modulations depend on the harmonics; thus, we apply the optimization to the low (67) and high (183) harmonics. One expects that the optimal energy modulations of other harmonics should be bounded between the results of these two harmonics.

GENESIS simulations are applied to the optimization process[27]. The input parameter to the EEHG optimizer is the targeted harmonic number. Then, the beamline parameters, $A_{1,2}$ and R_2, are predicted by the EEHG optimizer. Other parameters, $\lambda_{1,2}$ and R_1, are fixed. A 6D phase space distribution with the longitudinally bunched and transversely matched beam profile are generated as the GENESIS input. The transverse profile of the electron beam is determined by the NSLS-II lattice parameters in the short straight section, as shown in Table 2.

Relative energy spread σ_E/E	Beam energy E	Energy spread σ_E	x emittance ε_x	y emittance ε_y	I_{peak}	β_x	α_x	β_y	α_y	Radiator period λ_u
	MeV	MeV	m·rad	m·rad	A	m		m		cm
0.001	3000	3	$5.87\cdot10^{-6}$	$5.87\cdot10^{-8}$	300	3.77	0	4.20	0	6.40
* Normalized emittances are used										

Table 2. NSLS-II lattices and beam parameters include the Twiss at the short straight section and the RMS beam energy spread and normalized emittances.

3.1 Simulation of Harmonic 67

For the case of harmonic 67, the scaled energy modulation of stage 1 has been varied from 0.667 to 5.000. The evolutions of the peak power and the bunching factor through the undulator are plotted in Figs. 4a and 4b, respectively. One extreme is to start with a large initial bunching but at the expense of the large energy spread induced fast de-bunching, hence, less CR gain at the exit of the undulator. The other extreme is to begin with a small initial bunching that slowly increases through the undulator. In-between these two cases, there is an optimal initial energy modulation of stage 1, which is around $A_1=3.00$. The maximum bunching is achieved near the middle point of the undular length. Such optimized initial bunching allows a reasonably fast growth of the CR power as well as the bunching factor till the middle point of the undulator, then, the de-bunching process is mitigated and only mildly slows down the CR growth in the rest of the undulator, shown in Fig. 4a as the purple dashed line. The longitudinal phase spaces regarding these energy modulations of stage 1 with the values from 0.667 to 5.000 are shown in Figs. 5a to 5h, respectively. The final effective RMS energy spread, maximal bunching, momentum compaction of chicane 2, and energy modulation of stage 2 as a function of the energy modulation of stage 1 are plotted in Figs. 6a to 6d, respectively. From Fig. 6a, the optimal energy modulation $A_1=3$ brings 130% increase of the energy spread for the modulated beam slice. We will discuss how this increased slice energy spread influences other beamline experiments in Section 3.5.

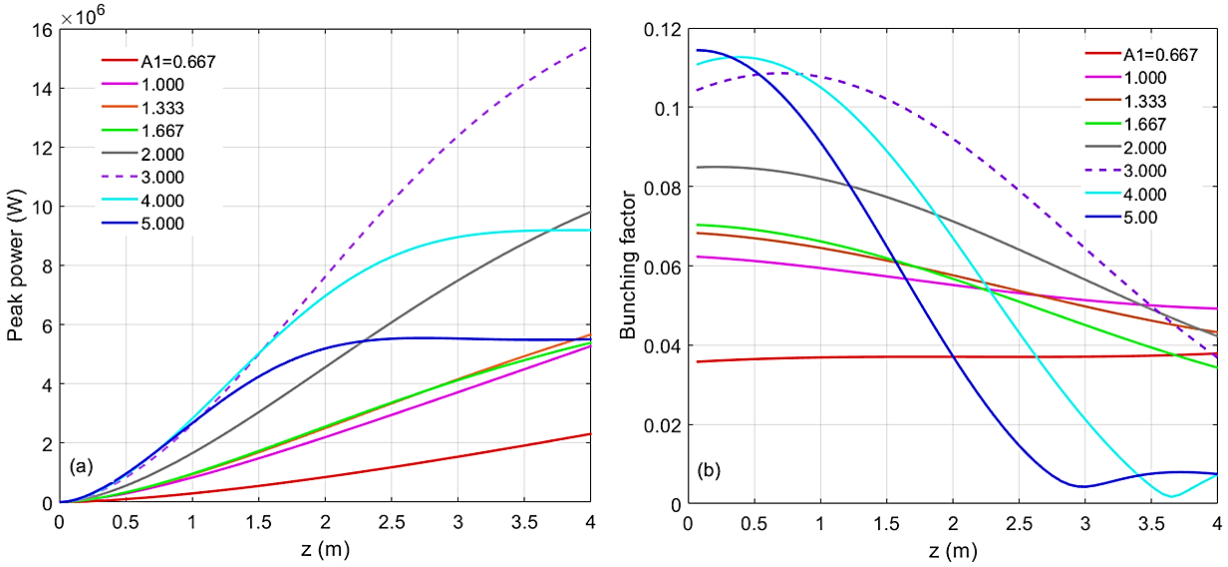

Figure 4. For the case of harmonic 67, the energy modulation of stage 1 is scanned with the values of 0.667 (red), 1.000 (magenta), 1.333 (orange), 1.667 (green), 2.000 (grey), 3.000 (purple), 4.000 (cyan), and 5.000 (blue). (a) Peak power vs undulator position. (b) Bunching factor vs undulator position.

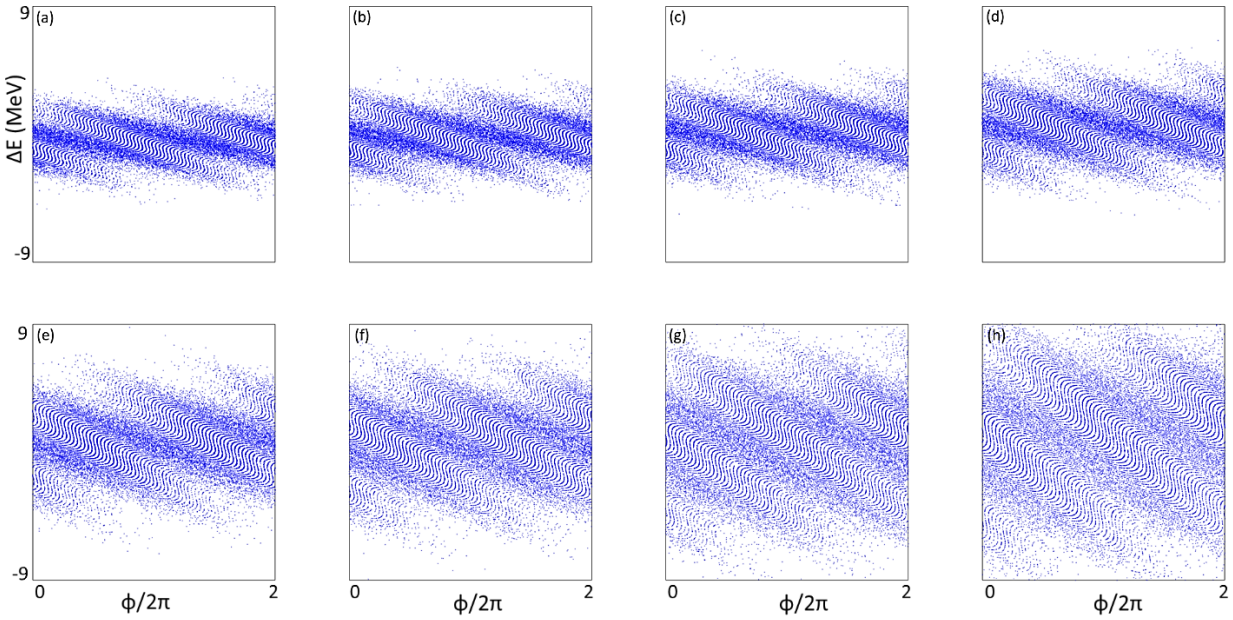

Figure 5. Longitudinal phase spaces corresponding to the energy modulations of stage 1 with the values of 0.667 (a), 1.000 (b), 1.333 (c), 1.667 (d), 2.000 (e), 3.000 (f), 4.000 (g), and 5.000 (h) are plotted respectively.

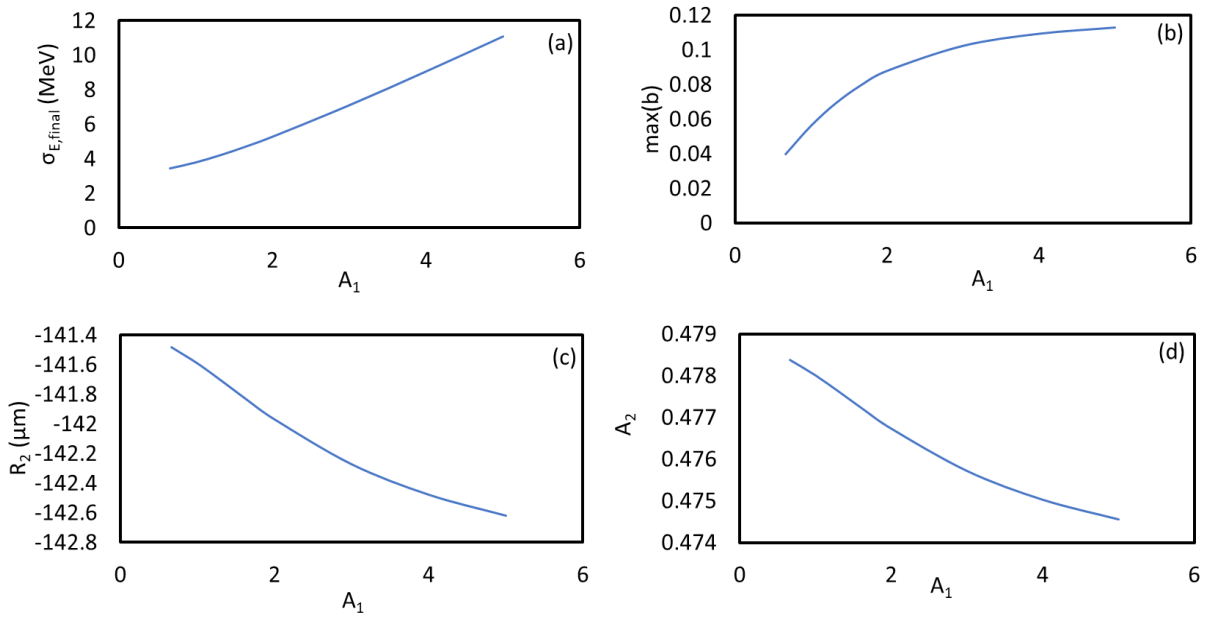

Figure 6. (a) The final effective RMS energy spread, (b) the maximal bunching, (c) the momentum compaction of chicane 2, and (d) the energy modulation of stage 2 as a function of the energy modulation of stage 1 are plotted, respectively.

3.2 Simulation of Harmonic 183

Similarly, for the case of harmonic 183, the energy modulation of stage 1 has been varied among the values from 0.667 to 5.000. Peak power and prebunching evolving through the undulator distance are plotted in Figs. 7a and 7b, respectively. The longitudinal phase spaces

corresponding to the energy modulations of stage 1 with the values from 0.667 to 5.000 are plotted in Figs. 8a to 8h, respectively. The final effective RMS energy spread, maximal bunching, momentum compaction of chicane 2, and energy modulation of stage 2 as a function of the energy modulation of stage 1 are plotted in Figs. 9a to 9d, respectively. The optimal energy modulation of stage 1 happens at A_1=2.00, which causes 95% increase of the energy spread for the modulated beam slice. As one expects, shorter the radiator wavelength is, less tolerance the de-bunching process has.

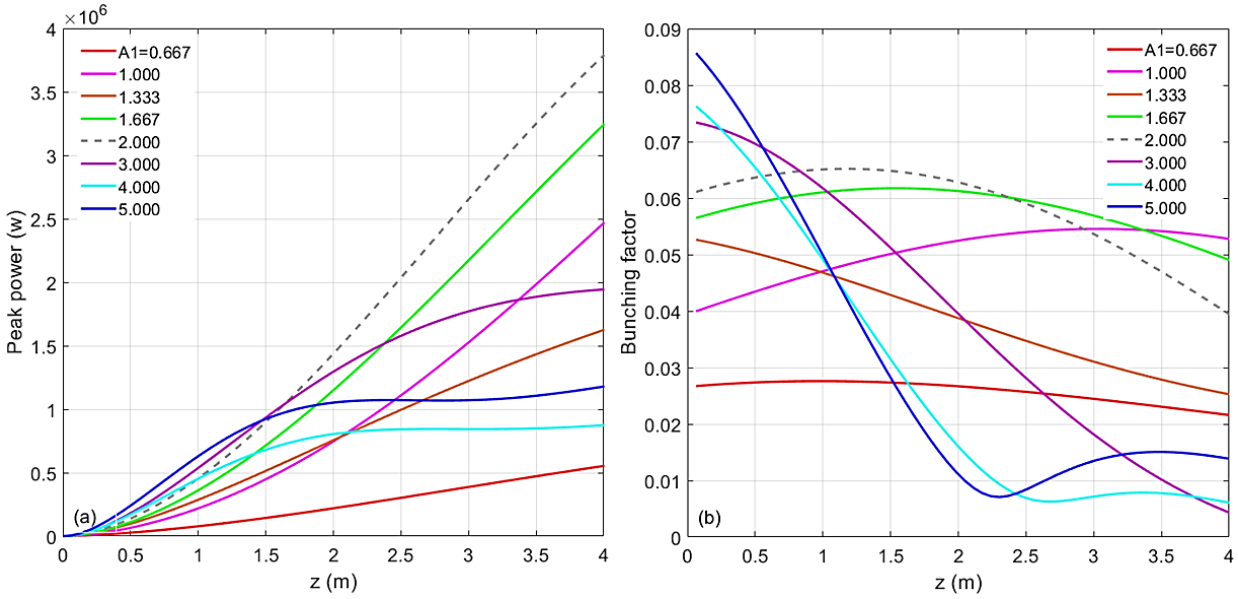

Figure .7 For the case of harmonic 183, the energy modulation of stage 1 is scanned with the values of 0.667 (red), 1.000 (magenta), 1.333 (orange), 1.667 (green), 2.000 (grey), 3.000 (purple), 4.000 (cyan), and 5.000 (blue). (a) Peak power vs undulator position. (b) Bunching vs undulator position.

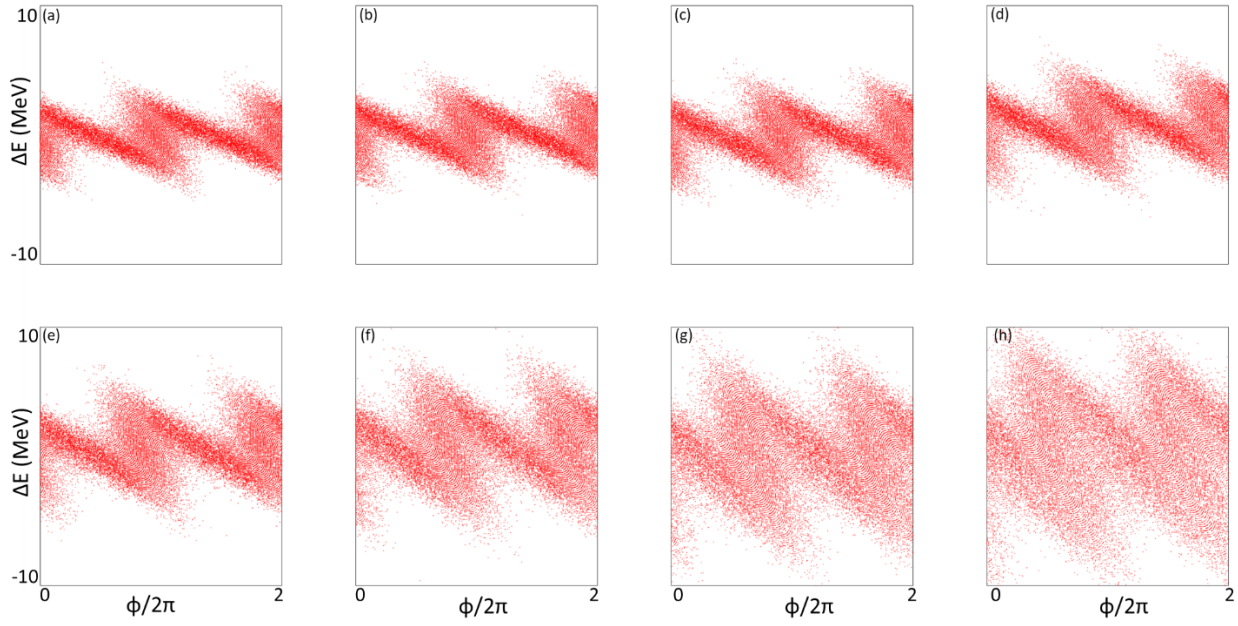

Figure 8. Longitudinal phase spaces corresponding to the energy modulations of stage 1 with the values of 0.667 (a), 1.000 (b), 1.333 (c), 1.667 (d), 2.000 (e), 3.000 (f), 4.000 (g), and 5.000 (h) are plotted.

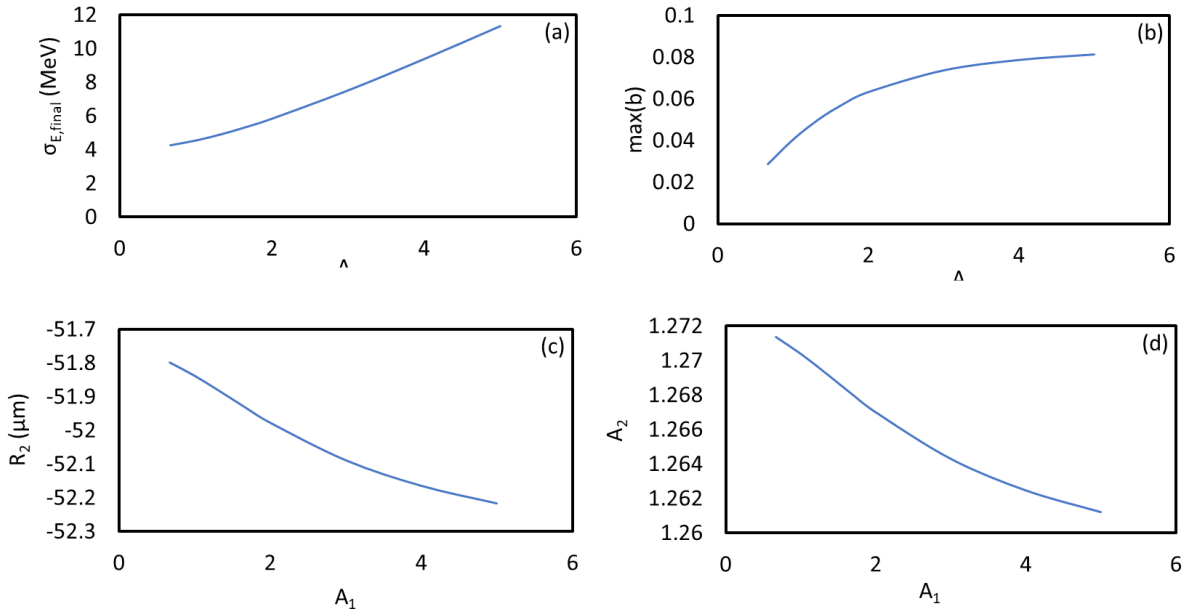

Figure 9. (a) The final effective RMS energy spread, (b) the maximal bunching, (c) the momentum compaction of chicane 2, and (d) the energy modulation of stage 2 as a function of the energy modulation of stage 1 are plotted, respectively.

3.3 Studies of Energy Spread Induced De-bunching

Usually, the energy modulation and the initial bunching factor are correlated. A higher energy modulation yields a higher initial bunching, but at the cost of a worse de-bunching effect. To solely study the energy spread induced de-bunching effect, we deliberately vary the effective energy spread while keeping the initial bunching constant. Larger initial energy spread causes faster de-bunching, which limits the CR power at the exit of the radiator. Higher harmonics usually require smaller energy modulation for a fixed undulator length. As one expects, the de-bunching becomes faster with the increase of the initial energy modulation. The optimal energy modulation happens while the maximum bunching is achieved in the middle point of the undulator length, shown as the red curves in Figs. 10a and 10b. Because the undulator is short and the initial bunching is substantial, FEL gain is not a concern and even higher harmonics can be produced until the de-bunching effect becomes strong for a length scale of about one meter.

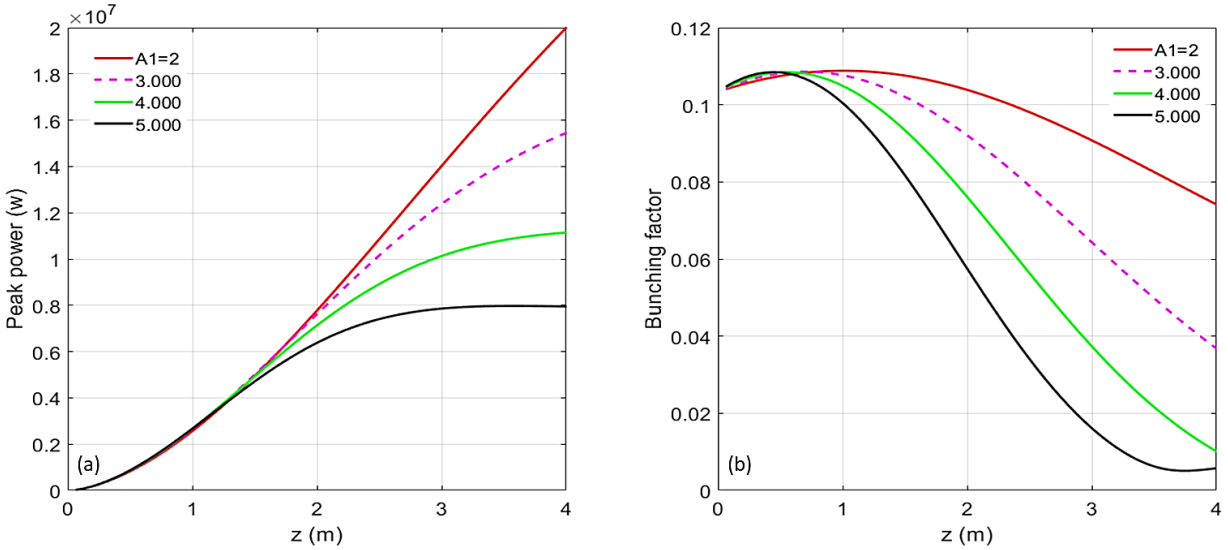

Figure 10. The energy modulation of stage 1 is scanned among the values of 2 (red), 3 (magenta), 4 (green), and 5 (grey) while the initial bunching is kept constant. (a) Peak power vs undulator position. (b) Bunching vs undulator position.

3.4 Laser Power and CR Properties

The required powers of laser 1 and laser 2 as functions of the harmonic number and the energy modulation of stage 1 are shown as the contour plots in Figs. 1e and 1f, respectively. Those required maximal laser powers, a few GW and ten GW regarding laser 1 and 2, can be achieved with the current laser technologies.

The CR is estimated for the shorter and longer wavelengths of carbon K-edge, 4.37 nm, and 11.94 nm, including the peak power, the number of photons per pulse, and the RMS spectral bandwidth regarding three different pulse durations in RMS, 0.43 ps, 0.85 ps, and 1.23 ps. For each case, those output properties are estimated in two different radiator lengths, 2.5 m, and 3.5 m, as shown in Table 3.

For the case of 3.5 m long radiator and 0.85 ps pulse duration, the maximum number of photons per pulse is $1.8 \cdot 10^{12}$ regarding 11.9 nm. The repetition rate can be up to 1 MHz, hence, the correspond spectral brightness is $1.3 \cdot 10^{21}$, which is more than two orders of magnitude higher than the current brightest source U (100) PMU (~ $1.1 \cdot 10^{19}$) at the NSLS-II[28,29].

T_{RMS} (ps)	P_{pk} at L_r = 2.5 m (MW)		Photon per pulse at L_r = 2.5 m		P_{pk} at L_r = 3.5 m (MW)		Photon per pulse at L_r = 3.5 m		RMS bandwidth		Spectral brightness at 1 MHz	
	λ_{67} =11.94 nm	λ_{183} =4.37 nm	λ_{67} =11.94 nm	λ_{183} =4.37 nm	λ_{67} =11.94 nm	λ_{183} =4.37 nm	λ_{67} =11.94 nm	λ_{183} =4.37 nm	λ_{67} =11.94 nm	λ_{183} =4.37 nm	11.94 nm	4.37 nm
0.426	10.14	2.03	$6.51 \cdot 10^{11}$	$4.77 \cdot 10^{10}$	14.2	3.27	$9.12 \cdot 10^{11}$	$7.69 \cdot 10^{10}$	$4.13 \cdot 10^{-5}$	$1.50 \cdot 10^{-5}$	$3.25 \cdot 10^{20}$	$7.54 \cdot 10^{19}$
0.851			$1.30 \cdot 10^{12}$	$9.54 \cdot 10^{10}$			$1.82 \cdot 10^{12}$	$1.54 \cdot 10^{11}$	$2.10 \cdot 10^{-5}$	$7.60 \cdot 10^{-6}$	$1.28 \cdot 10^{21}$	$2.98 \cdot 10^{20}$
1.277			$1.95 \cdot 10^{12}$	$1.43 \cdot 10^{11}$			$2.73 \cdot 10^{12}$	$2.31 \cdot 10^{11}$	$1.40 \cdot 10^{-5}$	$5.00 \cdot 10^{-6}$	$2.87 \cdot 10^{21}$	$6.78 \cdot 10^{20}$

Table 3. CR for the lower and upper wavelengths of carbon k-edge 4.37 nm and 11.94 nm, including the peak power, the number of photon pulse, and the RMS spectral bandwidth in three different pulse durations in RMS, 0.43 ps, 0.85 ps, and 1.23 ps are listed. For each case, those output properties are calculated at two different radiator lengths, 2.5 m, and 3.5 m.

3.5 Required Mode for EEHG

The EEHG scheme requires that the NSLS-II storage ring is operated at an alternative mode with one hundred 5 mA electron bunches, equally spaced around the ring. Such a 5-mA electron bunch has the RMS bunch length > 20 ps, thus, the modulated slice only occupies a few

percent of the entire bunch. Besides, the modulation only causes a local energy spread increase in the level of around 100%. One expects that the EEHG influences all other beamlines on the spectral brightness and the photon flux at the level of a few percent or less (this has been confirmed by Synchrotron Radiation Workshop simulations)[30], hence, most beamlines can simultaneously operate in this EEHG mode.

METHOD

Implementing EEHG optimizer with Ideal Performance

After m is chosen (usually to be -1)[8,9], setting the parameters is comparatively straightforward. The EEHG process produces microbunching at many different wavelengths, but wavelengths corresponding to different m are either far apart or yield negligible bunching at nearby harmonics. Thus, only one m for a given optimized configuration needs to be considered.

The ideal bunching at a given wavelength is $b_r = \langle \exp(-ic k_r t) \rangle$, and is given by

$$b_r = J_p(k_r R_2 \eta_{M2}) \cdot J_m(C \eta_{M1}) \cdot \exp\left(\frac{-1}{2} C^2 \sigma_\eta^2\right), \tag{4}$$

where

$$C = k_r R_2 + m k_1 R_1. \tag{5}$$

R_1 and R_2 are the two momentum compactions, and η_{M1} and η_{M2} are the amplitudes of the two energy modulations. This assumes an initial Gaussian energy distribution.

When $\eta_{M1} \gg \sigma_\eta$, the bunching has an optimal value of $|b_r| = \left| J_p(\pm j'_{p,1}) J_m(\pm \hat{j}_{m,1}) \right|$, where the arguments of the Bessel functions give the maximum values. Defining $A_{1,2} = \eta_{M1,2}/\sigma_\eta$, when A_1 is reduced and the exponential damping terms becomes relevant, the optimum bunch is given by

$$|b_r| = \left| J_p(\pm j'_{p,1}) J_m(\pm \hat{j}) \exp\left(\frac{-1}{2} \frac{\hat{j}^2}{A_1^2}\right) \right|, \tag{6}$$

where $j'_{p,1}$ is the location of the first maximum of the Bessel function J_p. A rough estimate for $\hat{j}$ is given by

$$\hat{j} \cong \frac{j'_{m,1}}{1 + \frac{\sigma_\eta^2}{\eta_{M1}^2}\left[1 - \left(\frac{m}{j'_{m,1}}\right)^2\right]^{-1}}. \tag{7}$$

A good asymptotic expansion for large values of p is

$$j'_{p,1} \cong p + 0.80861 \cdot p^{1/3} + 0.07249 \cdot p^{-1/3} - 0.05097 \cdot p^{-1}. \tag{8}$$

For the lowest indices (e.g., $p \le 10$), it is better to just use a table of values for $j'_{p,1}$; alternatively, the optimal settings can be calculated directly.

The final energy spread can approximately be given by

$$\sigma_{\eta f}^2 = \sigma_\eta^2 + \frac{1}{2} A_1^2 + \frac{1}{2} A_2^2. \tag{9}$$

To make EEHG effective, the value of C should be much smaller than the two terms $k_r R_2$ and $k_1 R_1$ (see Fig. 1c in Section 1.3). This is equivalent to requiring that $\eta_{M1} k_1 R_1 \gg 1$. There are two distinct solutions that generate the same bunching, since C can either be positive or negative, and either choice yields the same bunching (see Fig. 1i in Section 1.3). This is true even when all

dispersive sections have the normal sign for R_{56}. Comparing the form of optimization, we find $C = \pm \frac{\hat{j}}{\eta_{M1}}$, which implies

$$R_2 = \frac{C - m k_1 R_1}{k_r} = \frac{\pm \frac{\hat{j}}{\eta_{M1}} - m k_1 R_1}{k_r}, \tag{10}$$

$\eta_{M2} = \frac{j'_{p,1}}{k_r \cdot R_2}$.

The two optimal solutions have slightly different values for R_2 and A_2. The first term in R_2 is going to be small, so $R_2 \approx -\frac{m k_1 R_1}{k_r}$; however, such small correction cannot be ignored when evaluating C.

Based on these procedures, we have implemented EEHG optimizer for tuning all important parameters to achieve the ideal performance of an EEHG beamline in a synchrotron light source.

DISCUSSION

The EEHG seeding option could offer very narrow bandwidths and extremely high brightness, realized by diffraction-limited short pulses in transverse planes and Fourier-limited bandwidth in the EUV to soft X-ray spectrum. The attractive FEL features are negligible heat load on the beamline optics due to the narrow bandwidth and a potential capability to generate short pulses using a short pulse seeding. The advantage of a storage ring FEL compared to a linac-based one is much better pulse-to-pulse beam stability.

For the storage-ring-based EEHG FELs, we have implemented a complete set of tools, named EEHG optimizer, which can provide the optimized parameters for generating the longitudinal bunched and transverse matched 6D phase space distribution. Then, GENESIS simulation is applied to search the optimal energy modulation regarding each specific harmonic, aiming the highest CR gain as well as mitigated energy-spread induced de-bunching. This toolkit has been successfully applied to the NSLS-II storage ring as an example, with an up to two orders of magnitude improvement of the spectral brightness for the wavelength of 12 nm. Furthermore, the EEHG scheme can expand the capability of the NSLS-II with a fully coherent time-resolved tunable EUV and soft X-ray radiation source, also, such scheme is compatible with other beamlines with the minimum impact of NSLS-II routine operation. Compared to other storage-ring-based FELs, e.g., angular dispersion enhanced prebunching scheme for seeding coherent EUV and soft X-ray FEL[6,7,31-35], the EEHG approach holds a great promise, not only for its simplicity (no need of any lattice change) but also for the accessibility to much higher harmonics, toward the soft X-ray spectrum. This is because for the EEHG approach[8,9], the maximal bunching (b_n) decreases with the harmonic n as $n^{\frac{-1}{3}}$, as shown in Fig. 1g; instead, for the angular dispersion enhanced prebunching scheme[7], like HGHG, b_n decreases much faster with n, as n^{-1}. Thanks to our compact design, modulator 2 (1 m), chicane 2 (<0.5 m), and radiator (3.5 m) can all be fit into the 5 m short straight section.

Since the toolkit is designed and generalized to any type of a synchrotron light source based EEGH beamline, it can be easily extended to the 4th generation storage rings with the expected much better performances because of the diffraction-limited ultrasmall emittances.

There are usually three types of effects which can impact performance of an EEHG FEL. Wake fields and noise in the laser peak power can disrupt coherence of the output radiation pulse, although they should not impact the total power produced. Incoherent energy scatter can reduce the bunching and output power, but for the parameters used here this should not be a concern, in particular because of the large amplitude of the energy modulations required by the equilibrium energy spread. For a storage ring, however, there is also the possibility of collective effects disrupting the electron beam after many turns around the ring.

A combination of high bunch intensity and perturbations of the bunch over short scale lengths results in strong collective effects which may affect the electron bunch parameters. Beam interaction with the machine impedance can lead to bunch lengthening and excitation of the microwave instability which increases the energy spread. The bunch slicing will enhance the effects of coherent synchrotron radiation (CSR) including 3D emittance growth and possible excitation of the CSR burst instability. Quantitative analysis of the collective effects requires further investigation including extensive numerical simulations using specific parameters of the ring lattice, light-generating insertion devices, and vacuum chamber.

COMPETING INTERESTS

The authors declare no competing financial and non-financial interests in relation to the work described in the paper.

AUTHOR CONTRIBUTIONS

G. P. developed the EEHG optimizer. X. Y implemented a compact EEHG beamline design for a synchrotron light source using NSLS-II as example. X. Y. and G. P. developed the tool for generating the bunched beam distribution and performed the GENESIS simulation. X. Y. defined the criteria for optimizing the CR emission. X. Y. and G. P. prepared the figures. L. Y., V. S., T. S., G. P., and X. Y. contributed to the writing of the manuscript.

ACKNOWLEDGEMENTS

The authors are extremely grateful for the valuable discussion and great help from A. Cavalieri, L. Giannessi and W. Wan.

This work was supported by the Director, Office of Science, Office of Basic Energy Sciences, of the U.S. Department of Energy under Contract No. DE-AC02-05CH11231, and by Brookhaven National Laboratory Directed Research and Development Program, Projects No. 22-028. This manuscript has been authored by Brookhaven Science Associates under Contract No. DE-SC0012704 with the U.S. Department of Energy. The United States Government retains and the publisher, by accepting the article for publication, acknowledges that the United States Government retains a non-exclusive, paid-up, irrevocable, worldwide license to publish or reproduce the published form of this manuscript, or allow others to do so, for United States Government purposes.

DECLARATION

The datasets generated and analyzed during the current study are not publicly available due to the reason that we want to know who has an interest in our datasets but are available from the corresponding author on reasonable request.

REFERENCE

1. Yu, L. H., Generation of intense UV radiation by subharmonically seeded single-pass free-electron lasers, *Phys. Rev. A* **44**, 5178 (1991).
2. Yu, L. H., and Ben-Zvi, I., High-gain harmonic generation of soft x-rays with the "fresh bunch" technique, Nucl. Instrum. Methods Phys. Res., Sect. A 393, 96 (1997).
3. Yu, L. H., et al., High-Gain Harmonic-Generation Free-Electron Laser, Science 289, 932–934 (2000).
4. Yu, L. H., and Shaftan, T., Towards coherent X-ray free-electron lasers, Nature Photonics 13, 513-515 (2019).
5. Mitri, S. D., Cornacchia, M., Diviacco, B., Perosa, G., Sottocorona, F., and Spampinati, S., Bridging the gap of storage ring light sources and linac-driven free-electron lasers, Phys. Rev. Accel. Beams 24, 060702 (2021).
6. Feng, C., et al., Coherent extreme ultraviolet free-electron laser with echo-enabled harmonic generation, Phys. Rev. Accel. Beams 22, 050703 (2019).
7. Feng, C. and Zhao, Z., A Storage Ring Based Free-Electron Laser for Generating Ultrashort Coherent EUV and X-ray Radiation, *Sci. Rep*. **7**, 4724 (2017).
8. Stupakov, G., Using the Beam-Echo Effect for Generation of Short-Wavelength Radiation, *Phys. Rev. Lett.* **102**, 074801 (2009).
9. Xiang, D., and Stupakov, G., Echo-enabled harmonic generation free electron laser, *Phys. Rev. ST Accel. Beams* **12**, 030702 (2009).
10. Khan, S., *et al*., Generation of Ultrashort and Coherent Synchrotron Radiation Pulses at DELTA, Synchrotron Radiation News **26**, 25 (2013).
11. Willmott, P., An Introduction to Synchrotron Radiation: Techniques and Applications, 2nd Edition, Wiley, ISBN-10: 1119280397 (2019).
12. Mille, N., *et al.*, Ptychography at the carbon K-edge. *Commun Mater* **3,** 8 (2022).
13. Stiel, H., *et al*., Towards Understanding Excited-State Properties of Organic Molecules Using Time-Resolved Soft X-ray Absorption Spectroscopy. *Int. J. Mol. Sci*. **22**, 13463 (2021).
14. Segatta, F., Nenov, A., Orlandi, S., Arcioni, A., Mukamel, S. and Garavelli, M., Exploring the capabilities of optical pump X-ray probe NEXAFS spectroscopy to track photo-induced dynamics mediated by conical intersections, *Faraday Discuss*. **221**, 245–264 (2020).
15. Shaftan, T., Smaluk, V., and Wang, G., Concept of the complex bend, NSLS-II Technical Note No. 276, 2018.
16. Einfeld, D., Schaper, J., and Plesko, M., A lattice design to reach the theoretical minimum emittance for a storage ring, https://accelconf.web.cern.ch/e96/PAPERS/WEPG/WEP038G.PDF
17. Henderson, S., Status of the APS upgrade project, in Proceedings of IPAC-2015, Richmond, VA, USA (JACoW, Geneva, Switzerland, 2015), pp. 1791–1793, TUPJE067, http://accelconf.web.cern.ch/AccelConf/IPAC2015/papers/ tupje067.pdf.
18. Steier, C., Byrd, J., Nishimura, H., Robin, D., and Santis, S. D., Physics design progress towards a diffraction limited upgrade of the ALS, in Proceedings of IPAC2016, Busan, Korea (JACoW, Geneva, Switzerland, 2016), pp. 2956–2958, WWPOW049, https://accelconf.web.cern.ch/IPAC2016/papers/wepow049.pdf
19. Liu, L., Resende, X. R., and Rodrigues, A. R. D., Sirius (BR): A new Brazilian synchrotron light source, in Proceedings of IPAC-2016, Busan, Korea (JACoW, Geneva, Switzerland, 2010), pp. 2811–2814, WEPOW001, https://accelconf.web.cern.ch/IPAC10/papers/wepea006.pdf
20. Tavares, P. F., Bengtsson, J., and Andersson, Á., Future development plans for the MAX IV light source: Pushing further towards higher brightness and coherence, *J. Electron Spectrosc. Relat. Phenom*. **224**, 8 (2018).
21. Penn, G. and Reinsch, M., Designs and numerical calculations for echo-enabled harmonic generation at very high harmonics, Journal of Modern Optics 58, 1404-1418 (2011).

22. Penn, G., Stable, coherent free-electron laser pulses using echo-enabled harmonic generation, *Phys. Rev. ST Accel. Beams* **17**, 110707 (2014) .
23. Chao, A. W., Mess, K. H., Tigner, M., Zimmermann, F. Handbook of Accelerator Physics and Engineering, 2012.
24. Yu, L., Yang, X., Shaftan, T., Smaluk, V., Li, Y., Assessment of FEL options for NSLS-II upgrade, BNL LDRD # 22-028 (2022).
25. NSLS-II Conceptual Design Report: https://www.bnl.gov/isd/documents/75003.pdf
26. Halbach, K., Physical and Optical Properties of Rare Earth Cobalt Magnets, *Nucl. Instrum. and Methods* **187**, 109-117 (1981).
27. Reiche, S., GENESIS 1.3: A fully 3D time-dependent FEL simulation code, *Nucl. Instrum. Methods Phys. Res., Sect. A* **429**, 243 (1999).
28. NSLS-II Source Properties and Floor Layout (2010) https://www.bnl.gov/nsls2/docs/pdf/sourceproperties.pdf
29. Tanabe, T., NSLS-II Insertion Device Development, PAC07. https://indico.fnal.gov/event/1053/attachments/2236/2660/Toshiya_Tanabe_BNL.pdf
30. Chubar, O., *et al*., https://github.com/ochubar/SRW (2013).
31. Wang, X., *et al*., Angular dispersion enhanced prebunch for seeding ultrashort and coherent EUV and soft X-ray free-electron laser in storage rings, *J. Synchrotron Rad.* **26**, 677–684 (2019).
32. Li, C., et al., Lattice design for angular dispersion enhanced microbunching in storage rings, *JINST* **16**, 03004 (2021).
33. Nuhn, H.D., Tatchyn, R., Winick, H., Fisher, A.S., Gallardo, J.C., and Pellegrini, C., Short wavelength FELs on large storage rings, *Nucl. Instrum. Meth. A* **319** (1992) 89.
34. Mitri, S. D., and Cornacchia, M., Operating synchrotron light sources with a high gain free electron laser, *New J. Phys.* **17** (2015) 113006.
35. Zhao, Z. T., Storage ring light sources, *Rev. Accel. Sci. Tech.* **3** (2010) 57.